

Augmented Generator Sub-transient Model Using Dynamic Phasor Measurements

Pablo Marchi, Francisco Messina, Leonardo Rey Vega, Cecilia G. Galarza

Abstract—In this article, we present a new model for a synchronous generator based on phasor measurement units (PMUs) data. The proposed sub-transient model allows to estimate the dynamic state variables as well as to calibrate model parameters. The motivation for this new model is to use more efficiently the PMU measurements which are becoming widely available in power grids. The concept of phasor derivative is applied, which not only includes the signal phase derivative but also its amplitude derivative. Applying known non-linear estimation techniques, we study the merits of this new model. In particular, we test robustness by considering a generator with different mechanical power controls.

Index Terms—Synchronous generators, Modeling, PMU data, Unscented Kalman filter.

I. INTRODUCTION

DYNAMIC models form the basis for power system transient stability simulations. Simulation accuracy is driven, in part, by the accuracy of the individual models used to represent actual equipments installed in the field. Models are developed during the baseline testing in close coordination between the generator owner and manufacturer of the components. However, modeling errors exist in the dynamic studies used for planning and operating the bulk power system. These errors are introduced through component replacements, aging, measurement error, etc., that are not captured in these preliminary models. Some historical disturbances can partly be attributed to model inaccuracy. Post-mortem analyses using the ideal model from the planning stage have shown gross differences from actual performance [1]. Nowadays, the North American Electric Reliability Corporation (NERC) Reliability Standards MOD-026-1, MOD-027-1, MOD-032-1 and MOD-033-1 [2] seek to ensure that dynamic models remain within pre-defined limits so that they accurately represent the equipment installed in the field.

Traditionally, a short-circuit test on unloaded synchronous generator units offered the standard measure for transient parameters. However, due to its limitations on providing q-axis transient and sub-transient constants, several alternative tests, such as enhanced sudden short circuit test, stator decrement test and standstill frequency response test, have been

proposed for obtaining a better representation of the dynamic model [3]. Nevertheless, in practice, the implementation of these offline methods is inconvenient due to the high cost incurred when performing the disconnection of the generators. Recently, online methods have been proposed in order to assess the dynamic behavior, and to reduce the uncertainties, when the generator is working under stressful conditions. These techniques were designed to harness the measurements from Digital Fault Recorders (DFRs) installed at the point of connection [4].

The online methods can be separated in two groups depending on the type of data processing. The first one uses a frame-based processing approach. Some pioneering works on this matter are [5], [6]. In [5], the identification of synchronous generator reactances and time constants of the excitation system is achieved using a trajectory sensitivity method. In [6], nonlinear least squares estimation is applied to obtain a subset of the model parameters. With the inclusion of Phasor Measurement Units (PMUs), these techniques have evolved to include these new measurements. Among other advantages, these electronic devices record the electromechanical dynamics of the generating units with good precision and high reporting rates, which can reach up to 120 frames per cycle. That was how the second group of processing techniques arose. They are based on sample by sample Bayesian filtering, such as: the Extended Kalman Filter (EKF) [7], Unscented Kalman Filter (UKF) [8], Ensemble Kalman Filter (EnKF) [9], and Particle Filter (PF) [10].

The main objective of this paper is not to discuss which estimation technique is more adequate, but instead to analyze the model to be considered. Concretely, a sub-transient model is adopted and a new way of defining the transition function of the model is explained. It is worth mentioning that the sub-transient model was chosen with the criteria of including as many physical effects as possible. Thus, the performance of the estimates is improved by reducing the number of model uncertainties.

The main contributions of this work are:

- The presentation of a sub-transient generator model with the possibility of including the Automatic Voltage Regulator (AVR), the Power System Stabilizer (PSS) and the Turbine Governor (TG) control loops.
- A novel model that include not only voltage and current phasors, but also their time derivatives as well as the frequency and Rate Of Change Of Frequency (ROCOF).

The work of P. Marchi was supported by a CONICET Ph.D. grant. This work was partially funded by the UREE 4 FONARSEC project: “Development of Synchrophasor Measurements for Smart Electrical Grids”. The FONARSEC is funded by the Ministry of Science, Technology and Innovaton of Argentina.

P. Marchi, F. Messina, L. Rey Vega and C. G. Galarza are with the CSC-CONICET, and the School of Engineering - Universidad de Buenos Aires, Argentina (e-mail: pmarchi@csc.conicet.gov.ar, fmessina@fi.uba.ar, lrey@fi.uba.ar, cgalar@fi.uba.ar).

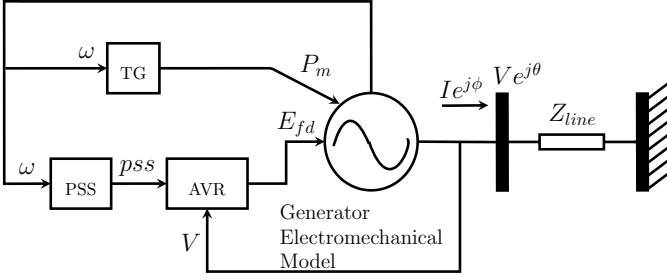


Fig. 1. Generator with controllers connected to an infinite bus.

The paper is organized as follows. Following a description of the model parameter estimation problem in Section II, we discuss the formulation of the sub-transient generator model in Section III. Section IV presents different scenarios to show the validity of the proposed method. Section V presents the conclusions and possible future work directions.

II. PROBLEM FORMULATION

A. Problem statement

The goal is to identify the model parameters as well as to dynamically estimate the internal states of a generator unit. To achieve this, measurements from a PMU at the point of connection will be used as inputs to the filtering algorithm. This type of technique is widely used and is known as *event playback* [11]. To introduce the subject, Fig. 1 shows a general structure of a power plant. The system consists of a synchronous generator, a TG, an AVR and a PSS.

B. Dynamic State Estimation

To estimate the dynamics of a generator unit, the general form of a state-space model for nonlinear systems is considered:

$$\begin{aligned} \mathbf{x}_k &= f_s(\mathbf{x}_{k-1}, \mathbf{u}_{k-1}) + \mathbf{w}_k, & \mathbf{x}_k &\in \mathbb{R}^n, \\ \mathbf{z}_k &= h_s(\mathbf{x}_k, \mathbf{u}_{k-1}) + \mathbf{v}_k. \end{aligned} \quad (1)$$

where f_s is the state transition function which models the generators dynamics, \mathbf{x} is the state vector, \mathbf{z} is the measurement vector, \mathbf{u} is the input vector, h_s is the function which relates the measurements with the state vector, and \mathbf{w} and \mathbf{v} are noise vectors introduced to account for modeling errors.

C. Review of Unscented Kalman Filter

Given its simplicity, its reduced computational cost, and its good performance for non-linear systems, we have adopted the UKF estimation algorithm. In addition, as it was shown in [10], the UKF is a feasible real time solution.

Unlike the well-known EKF, the UKF gets certain amount of extra terms from the Taylor series of f_s and h_s . Besides, it has not the necessity of computing the Jacobian of these functions. This algorithm defines the Unscented transformation to approximate the mean and covariance of the state vector. For this purpose, the concept of *sigma points* is introduced. These sigma points are propagated through the nonlinear functions and then the mean and the covariance

for \mathbf{x} ($\hat{\mathbf{x}}_k, P_k$) and \mathbf{z} ($\hat{\mathbf{z}}_k, H_k$) are approximated using a weighted sample mean and covariance of the posterior sigma points. Basically, the procedure can be divided in two steps: prediction and correction. Equations (2) to (5) summarize the filtering algorithm.

Select three positive scalars γ, β, κ and define the following constants:

$$\lambda = \gamma^2(n + \kappa) - n, \quad (2a)$$

$$w_0^m = \frac{\lambda}{n + \lambda}, \quad w_0^c = \frac{\lambda}{n + \lambda} + (1 - \gamma^2 + \beta), \quad (2b)$$

$$w_h^m = w_h^c = \frac{1}{2(n + \lambda)}, \quad h = 1, \dots, 2n. \quad (2c)$$

Prediction step:

Predicted (*a priori*) state estimate,

$$\hat{\mathbf{x}}_{k|k-1}^i = f_s \left(\hat{\mathbf{x}}_{k-1|k-1}^i, \mathbf{u}_{k-1} \right), \quad (3a)$$

$$\hat{\mathbf{x}}_{k-1|k-1}^0 = \hat{\mathbf{x}}_{k-1|k-1}, \quad (3b)$$

$$\hat{\mathbf{x}}_{k-1|k-1}^j = \hat{\mathbf{x}}_{k-1|k-1} + \left(\sqrt{(n + \lambda) P_{k-1|k-1}} \right)_j, \quad (3c)$$

$$\hat{\mathbf{x}}_{k-1|k-1}^{j+n} = \hat{\mathbf{x}}_{k-1|k-1} - \left(\sqrt{(n + \lambda) P_{k-1|k-1}} \right)_j, \quad (3d)$$

$$j = 1, \dots, n,$$

$$\hat{\mathbf{x}}_{k|k-1} = \sum_{i=0}^{2n} w_i^m \hat{\mathbf{x}}_{k|k-1}^i. \quad (3e)$$

Predicted (*a priori*) state covariance,

$$P_{k|k-1} = \tilde{P}_{k|k-1} + Q_k, \quad (4a)$$

$$\tilde{P}_{k|k-1} = \sum_{i=0}^{2n} w_i^c \left(\hat{\mathbf{x}}_{k|k-1}^i - \hat{\mathbf{x}}_{k|k-1} \right) \left(\hat{\mathbf{x}}_{k|k-1}^i - \hat{\mathbf{x}}_{k|k-1} \right)^T. \quad (4b)$$

Correction step:

$$\hat{\mathbf{z}}_{k|k-1}^i = h_s \left(\hat{\mathbf{x}}_{k|k-1}^i, \mathbf{u}_{k-1} \right), \quad (5a)$$

$$\hat{\mathbf{z}}_{k|k-1} = \sum_{i=0}^{2n} w_i^m \hat{\mathbf{z}}_{k|k-1}^i, \quad (5b)$$

$$\tilde{\mathbf{y}}_k = \mathbf{z}_k - \hat{\mathbf{z}}_{k|k-1}, \quad (5c)$$

$$H_k = \sum_{i=0}^{2n} w_i^c \tilde{\mathbf{y}}_k \tilde{\mathbf{y}}_k^T, \quad (5d)$$

$$K_k = P_{k|k-1} H_k^T \left(H_k P_{k|k-1} H_k^T + R_k \right)^{-1}, \quad (5e)$$

$$\hat{\mathbf{x}}_{k|k} = \hat{\mathbf{x}}_{k|k-1} + K_k \tilde{\mathbf{y}}_k, \quad (5f)$$

$$P_{k|k} = \left(I - K_k H_k \right) P_{k|k-1}. \quad (5g)$$

Here, the estimate of the state vector at time k is computed using the measurements at time l and is denoted as $\hat{\mathbf{x}}_{k|l}$, $\hat{\mathbf{x}}_{l|m}^i$ and $\hat{\mathbf{z}}_{l|m}^i$ are the sigma points of the state vector and the measurements respectively $\forall i = 0, \dots, 2n$, R_k is the measurement noise covariance matrix at time k , Q_k the process noise covariance matrix at time k , and the $(\cdot)_j$ operator takes the j -th row of the matrix. For an in-depth discussion, please refer to [8].

III. DYNAMIC GENERATOR MODELING

A. Conventional Sub-transient Generator Model

The transient model is the simplest model that allows to add control loops into the mechanical power and field voltage. Because of that, it is widely used [10], [12], [13]. However, the sub-transient model is more complete since it incorporates to the transient model a new set of time constants (T'_d , T''_q) that define faster electromagnetic changes. The model was introduced for calibration purposes in [11], but only the rotor equations were considered. In this paper, all the effects modeled in the Power System Toolbox (PST) [14] are taken into account. This analysis lays the basis for the model that will be introduced in Section III-B. Consider the following set of equations expressed in the per-unit (p.u.) system:

Electromechanical equations:

$$\frac{d\delta}{dt} = \omega_s (\omega - \omega_0), \quad (6a)$$

$$\frac{d\omega}{dt} = \frac{\omega_0}{2H} [P_m - T_e - D (\omega - \omega_0)]. \quad (6b)$$

Subtransient rotor equations:

$$\frac{dE'_d}{dt} = \frac{1}{T'_q} [-E_d - k_2 (E'_d - \Psi_q) - k_1 I_q], \quad (7a)$$

$$\frac{dE'_q}{dt} = \frac{1}{T'_d} [E_{fd} - S(E'_q) - k_3 (E'_q - \Psi_d) - k_4 I_d], \quad (7b)$$

$$\frac{d\Psi_d}{dt} = \frac{1}{T''_d} [-\Psi_d + E'_q - (x'_d - x_{ls}) I_d], \quad (7c)$$

$$\frac{d\Psi_q}{dt} = \frac{1}{T''_q} [-\Psi_q + E'_d - (x'_q - x_{ls}) I_q]. \quad (7d)$$

AVR equations:

$$\frac{dE_{fd}}{dt} = \frac{1}{T_A} [-E_{fd} + K_A (pss + V_{REF} - V_{TR})], \quad (8a)$$

$$\frac{dV_{TR}}{dt} = \frac{1}{T_R} (V - V_{TR}). \quad (8b)$$

TG equation:

$$\frac{dP_m}{dt} = \frac{1}{T_{ef}} \left[-P_m + (1 - \omega) \frac{1}{r} + P_{m,0} \right]. \quad (9)$$

To complete the system, additional equations are given in Appendix A. A full description of the notation is given in Appendix B. The model presented above can be found in [15]. As in [13] the AVR was modeled as a proportional-integral control, and the transducer effect has been taken into account. Unlike [8] and [13], the TG equation only considers a simple pole defined by an effective time constant T_{ef} . This consideration will be discussed later. To simplify the exposition, the PSS was modeled as a constant. Alternatively, its output could be included in (8a).

To select the parameters of the generator to be estimated we refer to the sensitivity analysis carried out in [16], and corroborated by [11]. These *key parameters* will be those whose deviations produce greater changes in the delivered active and reactive power. Thus, the parameters to estimate are the inertia constant and the exciter gain, defining the parameter

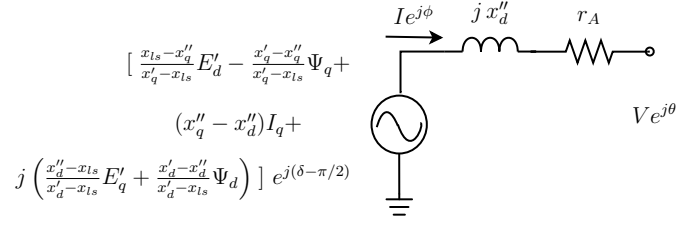


Fig. 2. Synchronous machine sub-transient dynamic circuit model.

vector to calibrate $\mathbf{x}_{cal} = [H, K_A]$. Therefore, the state vector is defined as:

$$\mathbf{x} = [\delta \ \omega \ E'_d \ E'_q \ \Psi_d \ \Psi_q \ E_{fd} \ V_{TR} \ P_m \ \mathbf{x}_{cal}]^T, \quad (10)$$

and $\dot{\mathbf{x}}_{cal} = \mathbf{0}$ is used to complete the specification of f_s .

Using the same criteria as in [10], the measurement vector is composed of the real and imaginary parts of the voltage phasor:

$$\mathbf{z} = [V_{re} \ V_{im}]^T. \quad (11)$$

Under this criteria, \mathbf{z}_k will contain an associated noise whose distribution corresponds to the distribution of the error in the voltage phasor measurement. To relate these measurements to the state vector, the electrical interface for this type of models is used (see Fig. 2). Using the following definitions:

$$\Psi''_q = \frac{x_{ls} - x''_q}{x'_q - x_{ls}} E'_d - \frac{x'_q - x''_q}{x'_q - x_{ls}} \Psi_q,$$

$$\Psi''_d = \left(\frac{x''_d - x_{ls}}{x'_d - x_{ls}} E'_q + \frac{x'_d - x''_d}{x'_d - x_{ls}} \Psi_d \right),$$

and assuming that $x''_q \approx x''_d$, the current flow through the branch can be expressed as:

$$I e^{j\phi} = \frac{(\Psi''_q + j\Psi''_d) e^{j(\delta - \pi/2)} - V e^{j\theta}}{r_A + jx''_d}. \quad (12)$$

After some manipulations, the measurements equations are:

$$V_{re} = \Psi''_q \sin(\delta) + \Psi''_d \cos(\delta) + I_{im} x''_d - I_{re} r_A, \quad (13a)$$

$$V_{im} = -\Psi''_q \cos(\delta) + \Psi''_d \sin(\delta) - I_{re} x''_d - I_{im} r_A. \quad (13b)$$

The resulting h_s can be obtained from (13). At last, the control vector necessary to stabilize the system will be composed by the following signals:

$$\mathbf{u} = [P_e \ I_{re} \ I_{im}]^T. \quad (14)$$

B. Augmented Sub-transient Generator Model

The idea is to extend the conventional model to include the frequency and the ROCOF measurements given by the PMUs. The standard definition of this quantities can be found in [17]. In this way, we would expect that this model would increase the observability of the closed loop system. But the state variables are hard to relate with the measured frequency and ROCOF. Note that the value of these measurements depend on the dynamics of all the generators and associated loads in the entire power system. As our main interest is to perform the calibration procedure in a decoupled way, no accurate model

can be proposed. However, as all the generators have internal impedances much smaller than the equivalent impedance of the rest of the network, the approximation given by (15) can be made. From now on, the ROCOF is denoted as α .

$$f \approx \omega, \quad \alpha \approx \dot{\omega}. \quad (15)$$

Accordingly, the new measurement vector is defined as:

$$\mathbf{z} = [V_{re} \ V_{im} \ f \ \alpha]^T. \quad (16)$$

Now, the function h_s is defined using (13) and (15). Note that the quality of this approximation can be controlled by the selection of R_k . Besides, it is concluded that the variable $\dot{\omega} = \frac{d\omega}{dt}$ should be added to the state vector. To achieve this, the transition equation (6b) should be modified:

$$\frac{d\omega}{dt} = \dot{\omega}, \quad (17a)$$

$$\frac{d\dot{\omega}}{dt} = \frac{\omega_0}{2H} \left(\dot{P}_m - \dot{T}_e - D\dot{\omega} \right). \quad (17b)$$

where, from (36c), we obtain:

$$\dot{T}_e = \dot{P}_e + r_A \left(2I_d \dot{I}_d + 2I_q \dot{I}_q \right). \quad (18)$$

By definition, and after differentiation we get:

$$P_e = \text{Re} \{S\} = \text{Re} \{V e^{j\theta} I e^{-j\phi}\} = V I \cos(\theta - \phi), \quad (19)$$

$$\dot{P}_e = \left(\dot{V} I + V \dot{I} \right) \cos(\theta - \phi) - V I \sin(\theta - \phi) \left(\dot{\theta} - \dot{\phi} \right). \quad (20)$$

Now, the term of the derivative of the electrical torque which contains the losses of the armature resistance is analyzed. Taking into account (36a) and (36b), we obtain:

$$\dot{I}_d = \left(\dot{I}_{re} + I_{im} \omega \right) \sin(\delta) + \left(I_{re} \omega - \dot{I}_{im} \right) \cos(\delta), \quad (21)$$

$$\dot{I}_q = \left(\dot{I}_{im} - I_{re} \omega \right) \sin(\delta) + \left(I_{im} \omega + \dot{I}_{re} \right) \cos(\delta). \quad (22)$$

From (18), (21) and (22), and after some simplifications we get:

$$\dot{T}_e = \dot{P}_e + 2r_A \left(I_{re} \dot{I}_{re} + I_{im} \dot{I}_{im} \right). \quad (23)$$

From (17b), we see that this model works with \dot{P}_m , instead of P_m , so (9) is replaced by:

$$\frac{d\dot{P}_m}{dt} = \frac{1}{T_{ef}} \left[-\dot{P}_m - \dot{\omega} \frac{1}{r} \right]. \quad (24)$$

If it is necessary to estimate P_m , the state vector \mathbf{x} should be augmented again to include this new variable. Finally, the new control and state vectors are defined as:

$$\mathbf{x} = \left[\delta \ \omega \ \dot{\omega} \ E'_d \ E'_q \ \Psi_d \ \Psi_q \ E_{fd} \ V_{TR} \ \dot{P}_m \ \mathbf{x}_{cal} \right]^T, \quad (25)$$

$$\mathbf{u} = \left[\vec{V} \ \vec{I} \ \vec{V} \ \vec{I} \right]^T. \quad (26)$$

This model has three advantages:

- The model does not depend on the mechanical power value in steady state $P_{m,0}$. In the literature, this value, as well as others parameters from TG detailed models, are

assumed to be known. Nevertheless, in practice, this is not always the case.

- The calibration process is more robust. This can be recognized by inspecting (6b) and (17b). In both equations the variable H is involved. In the first equation P_m and T_e are comparable magnitudes while in the last one \dot{P}_m and \dot{T}_e are not. In fact, \dot{P}_m is always much smaller than \dot{T}_e . Accordingly, it is expected that this improvement could handle more sophisticated models without knowledge of the structure of the TG or its parameters.
- By including the phasor derivatives at the input, the model gives more details of the dynamics of the rotor. Indeed, for a judiciously chosen description of the measurement noise, the estimates depend more on the transition model than on the measurement one. As a consequence, the approximation given by (15) becomes less relevant.

C. Phase and magnitude derivatives

The PMU or DFR should be capable of measuring all the variables involved in (20). Beyond the fact that some of these magnitudes are not defined by the aforementioned standards, it is well known that there are several algorithms for phasor estimation which estimate the phasor and its first and second derivatives [18]–[21]. From the phasor derivatives, it is possible to compute the derivatives for amplitude and phase in (20). If the voltage phasor is a complex number defined as $\vec{V} = V_{re} + jV_{im} = V e^{j\theta}$, then:

$$\dot{\vec{V}} \equiv \frac{d\vec{V}}{dt} = \left(\frac{dV}{dt} + jV \frac{d\theta}{dt} \right) e^{j\theta}, \quad (27)$$

$$\frac{\dot{\vec{V}}}{\vec{V}} = \frac{\dot{V}}{V} + j \frac{d\theta}{dt}. \quad (28)$$

The same procedure is followed for the current phasor $\vec{I} = I_{re} + jI_{im} = I e^{j\phi}$, and the following expressions are obtained:

$$\begin{cases} \frac{dV}{dt} = V \text{Re} \left\{ \frac{\dot{\vec{V}}}{\vec{V}} \right\} \\ \frac{d\theta}{dt} = \text{Im} \left\{ \frac{\dot{\vec{V}}}{\vec{V}} \right\} \end{cases}, \quad \begin{cases} \frac{dI}{dt} = I \text{Re} \left\{ \frac{\dot{\vec{I}}}{\vec{I}} \right\} \\ \frac{d\phi}{dt} = \text{Im} \left\{ \frac{\dot{\vec{I}}}{\vec{I}} \right\} \end{cases} \quad (29)$$

IV. NUMERICAL RESULTS

As it was mentioned before, the PST toolbox is used to perform all the simulations. The classical two-area and four machine system shown in Fig. 3 is the system to be considered. From the PST output, the measurements of a PMU located at the bus number 1 are generated. These measurements include the voltage and current phasors, their time derivatives, the frequency, and the ROCOF. All of them are computed considering a reporting rate of $f_r = 60$ fps and an additive white Gaussian noise (AWGN). This AWGN condition can be achieved using a preprocessing of the data, as is shown in [22], so that this assumption is not as strong as it seems. Then, the adjustment of the noise variance is made. It guarantees the following values for the standard metrics:

$$\text{TVE} = 1\%, \quad \text{FE} = 5 \text{ mHz}, \quad \text{RFE} = 0.1 \text{ Hz/s}. \quad (30)$$

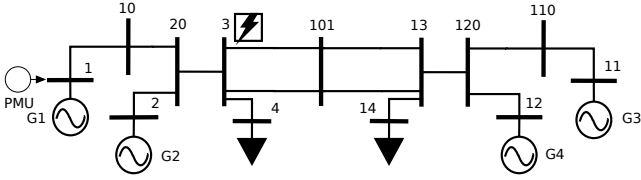


Fig. 3. Single line diagram of the test system.

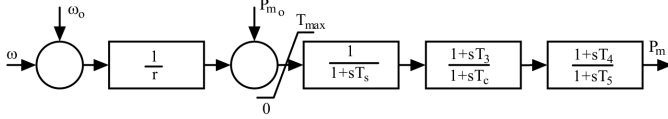


Fig. 4. Simple turbine governor model.

In this manner, the measurement covariance matrix is defined:¹

$$R_k = \text{diag} \{ [\sigma_{V_{re}}^2 \sigma_{V_{im}}^2 \sigma_f^2 \sigma_\alpha^2] \}. \quad (31)$$

The voltage noise is complex and circularly-symmetric, i.e., $\sigma_{V_{re}} = \sigma_{V_{im}} = |\vec{V}| \text{TVE}/(3\sqrt{2})$, and assuming $|\vec{V}| \approx 1$ p.u. The values of σ_f and σ_α were chosen from Monte Carlo simulations under realistic conditions, and they result to be $\sigma_f = \sigma_\alpha = \sqrt{10^{-5}}$.

Samples are interpolated to reduce the effect of the system nonlinearities in the filtering stage. A linear interpolation is chosen with the following interpolation factor $k_{int} = 16$. So, the time between samples results in: $\Delta t = 1.042 \times 10^{-3}$ s. The results presented above were obtained by proposing a realistic initial condition:

$$\mathbf{x}_0 = [1.1\theta_0 \ f_0 \ \alpha_0 \ 1 \ 1 \ 1 \ 1 \ 1 \ 1 \ 1 \ 0 \ 0.8H \ 0.6K_A]^T, \quad (32)$$

where θ_0 , f_0 and α_0 are the phasor phase, the frequency and the ROCOF measurements 33ms after the fault is cleared. At this time, the large nonlinearities are reduced and the calibration process starts. Then, with this configuration, the following state covariance matrix and process noise covariance are defined as:

$$Q_k = 10^{-10} \Delta t \ I, \quad P_0 = \text{cov}(\mathbf{p}), \quad (33)$$

$$\mathbf{p} \sim \mathcal{U}(\mathbf{x}_{0\text{ref}} - \Delta\mathbf{x}_0, \mathbf{x}_{0\text{ref}} + \Delta\mathbf{x}_0), \quad (34)$$

where $\mathbf{x}_{0\text{ref}}$ is the reference value of the state vector at the start time, $\Delta\mathbf{x}_0 = |\mathbf{x}_{0\text{ref}} - \mathbf{x}_0|$ where $|\cdot|$ is the componentwise absolute value function, \mathbf{p} is a random vector with uniform distribution and independent components, and I is the identity matrix of 12×12 . Finally, the selected parameters of the UKF are $\gamma = 10^{-3}$, $\beta = 2$, $\kappa = 0$.

A. Scenario A

A three-phase line to ground fault is applied in the bus number 3 at $t = 0.1$ s. After another 100ms the fault is cleared and the system starts an oscillatory process. A sub-transient

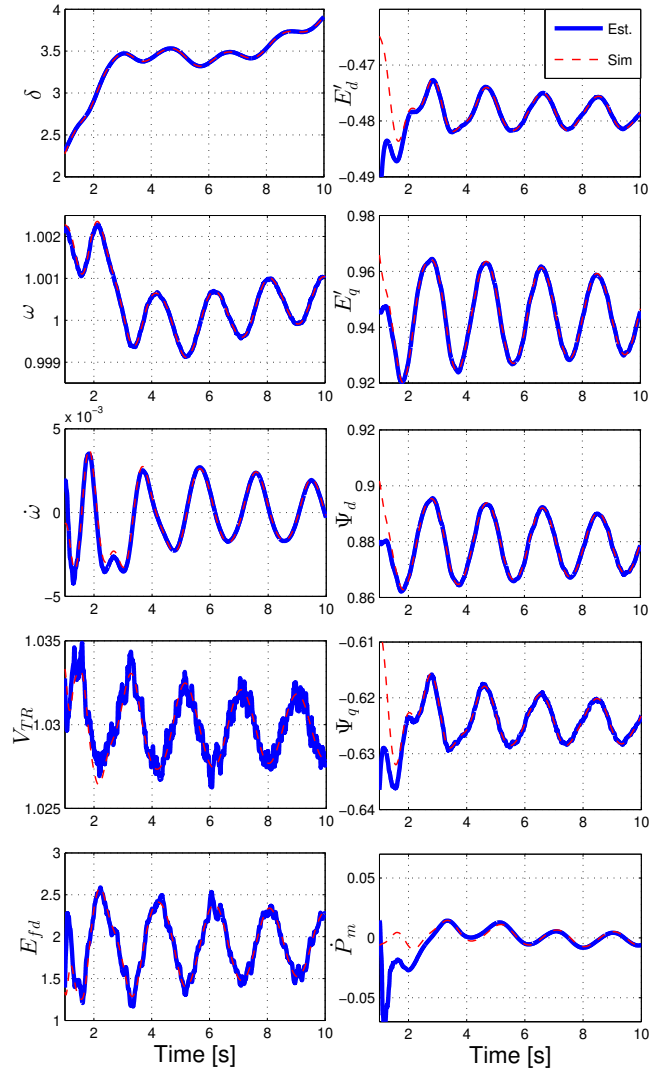


Fig. 5. Scenario A: Estimated dynamic states as a function of time.

generator model for all generators is assumed (concretely the parameters used in the *d2asbeg.m* PST example file). Using the model described in Section III-A, all the equations are matched with the simulator, except for the TG equations. For this subsystem PST considers a more sophisticated model that can be observed in Fig. 4. As it can be seen, the transfer function of this subsystem implies more than one single pole. Several other parameters are included. From the transfer function, the associated cutoff frequency is calculated and the value of T_{ef} is determined ($T_{ef} = 2.4$ s). Using the model presented in Section III-B the UKF is implemented, and the results are displayed in Fig. 5 and 6. It can be observed, that despite the noise added to the measurements and the poor initialization of the system, the dynamic state variables and the generator parameters are tracked with a good degree of accuracy.

B. Scenario B

In order to evaluate the performance of a multiple generator calibration procedure, we propose to repeat the previous simulation for each one of the generator units (G1-G4), with

¹Note that $\text{diag}\{\mathbf{d}\}$ is a diagonal matrix with diagonal elements from \mathbf{d} and the operator $\text{cov}(\mathbf{d})$ is the covariance matrix of the random vector \mathbf{d} .

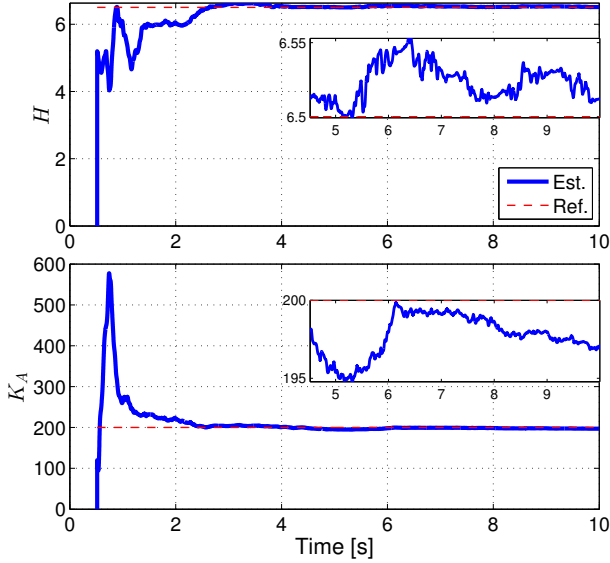


Fig. 6. Scenario A: Calibrated parameters as a function of time. A zoom of the state variable after convergence is included.

TABLE I
DIFFERENCE IN % WITH RESPECT TO THE REFERENCE PARAMETER.

	G1	G2	G3	G4
H_0	-20	15	50	-40
K_{A0}	-40	50	15	-20

the same calibration parameters. As in the previous case, the initialization of the dynamic variables is maintained, but the selection of the initial uncalibrated parameters is carried out arbitrarily, as detailed in Table I. We perform a Monte Carlo simulation using the model of Section III-B, and we compare the results with other in the literature [10]. For that, the mean square error (MSE) is used as a metric.

$$\text{MSE}(\hat{x}_k^j) = \frac{1}{M} \sum_{m=1}^M \left(\hat{x}_{k,m}^j - x_{k,\text{ref}}^j \right)^2, \quad j = 1, \dots, n, \quad (35)$$

where $M = 100$ is the number of Monte Carlo trials when the estimated MSEs did not change significantly, $\hat{x}_{k,m}^j$ is the j -th component of the state vector estimate at time k and m -th realization, and $x_{k,\text{ref}}^j$ is the true value of the state at the same time. Then, worst case of the MSEs after convergence is considered. To increase the dynamic range, $\text{MSE}[\text{dB}] = 10 \log_{10}(\text{MSE})$ is used to display the results in Tables II to V. The model of Section III-A can be contrasted against the one presented in Section III-B. To make a fair

TABLE II
SCENARIO B: MEAN AND STANDARD DEVIATION OF THE ESTIMATED PARAMETERS ($H = 6.5, K_A = 200$), USING THE CONVENTIONAL MODEL.

	G1	G2	G3	G4
\bar{H}	7.3939	8.0854	1.8318	7.0461
s_H	0.24177	0.34196	11.312	0.1473
\bar{K}_A	182.29	188.5	198.67	190.28
s_{K_A}	3.8452	2.1438	26.806	2.5905

TABLE III
SCENARIO B: MSE [dB], USING THE CONVENTIONAL MODEL.

State	G1	G2	G3	G4
δ	-43.715	-44.197	95.82	-42.017
ω	-74.615	-74.94	15.221	-73.68
E'_d	-66.845	-69.245	-23.005	-69.665
E'_q	-61.97	-64.755	-17.573	-66.145
Ψ_d	-57.705	-60.275	-18.218	-63.04
Ψ_q	-58.215	-59.47	-20.905	-58.175
V_{TR}	-51.835	-53.62	-18.529	-52.82
E_{fd}	-15.415	-15.489	-5.917	-13.448
P_m	-36.189	-36.155	52.265	-36.272

TABLE IV
SCENARIO B: MEAN AND STANDARD DEVIATION OF THE ESTIMATED PARAMETERS ($H = 6.5, K_A = 200$), USING THE AUGMENTED MODEL.

	G1	G2	G3	G4
\bar{H}	6.6214	6.5513	6.1415	6.0334
s_H	0.043687	0.12926	0.14719	0.16517
\bar{K}_A	197.36	197.18	197.47	197.2
s_{K_A}	2.2053	2.0048	2.1607	2.1406

comparison, a 2% deviation of the value of the $P_{m,0}$ was added in the TG equation, which is an optimistic assumption, considering that the value in principle is unknown and it will always have an associated error. It is clear that for some realizations, the estimation based on the model G3 may be unstable. This will not be the case for the augmented model described in Section III-B.

It is relevant to analyze the output of the calibrated system and compare it with the one that is non-calibrated. In this context, the active (P_e) and reactive powers (Q_e) from G1 have been plotted in Fig. 7. The label Cal 1 refers to estimates using the model described in Section III-A, while the label Cal 2 is reserved for the results from the augmented model. Again, the differences of the results are notorious.

C. Scenario C

Finally, the TGs of all the generators are modified to test robustness against different models. Now, the Hydro-turbine

TABLE V
SCENARIO B: MSE [dB], USING THE AUGMENTED MODEL.

State	G1	G2	G3	G4
δ	-57.88	-59.975	-61.935	-61.36
ω	-91.205	-93.635	-94.86	-94.2
$\dot{\omega}$	-83.515	-83.2	-81.515	-80.42
E'_d	-74.725	-74.5	-74.495	-74.31
E'_q	-64.87	-64.71	-64.85	-64.44
Ψ_d	-66.14	-66.105	-65.98	-65.01
Ψ_q	-70.375	-69.635	-69.165	-69.055
V_{TR}	-67.475	-66.965	-64.58	-65.09
E_{fd}	-23.325	-25.314	-24.484	-24.208
\dot{P}_m	-72.885	-74.265	-66.815	-71.165

TABLE VI
SCENARIO C: MEAN AND STANDARD DEVIATION OF THE ESTIMATED
PARAMETERS ($H = 6.5, K_A = 200$), USING THE AUGMENTED MODEL.

	G1	G2	G3	G4
\bar{H}	6.6229	5.7946	6.2957	6.4214
s_H	0.09272	0.37598	0.133	0.20374
\bar{K}_A	202.73	203.1	203.08	202.84
s_{K_A}	2.2093	2.2296	2.2904	2.0347

TABLE VII
SCENARIO C: MSE [dB], USING THE AUGMENTED MODEL.

State	G1	G2	G3	G4
δ	-60.79	-55.185	-58.575	-58
ω	-96.505	-85.665	-91.665	-90.74
$\dot{\omega}$	-86.69	-71.6	-79.15	-77.575
E'_d	-75.37	-75.38	-74.305	-75.235
E'_q	-65.02	-66.17	-64.73	-65.97
Ψ_d	-66.16	-68.335	-66.385	-66.875
Ψ_q	-69.925	-68.85	-68.57	-69.185
V_{TR}	-66.35	-65.99	-64.165	-65.315
E_{fd}	-25.037	-22.489	-23.586	-23.295
\dot{P}_m	-64.515	-64.295	-59.86	-60.495

model showed in Fig. 8 is selected (the parameters can be found in the PST example file *d2asbegh.m*). It is clear that it presents a degree of complexity even more advanced than in the previous case. Without changing T_{ef} or any initialization of the system, tables VI and VII show the new results. Notice that performance is not significantly degraded.

V. CONCLUSIONS

In this paper, we have introduced a new state variable model for a generator unit based on PMU data. For that, we

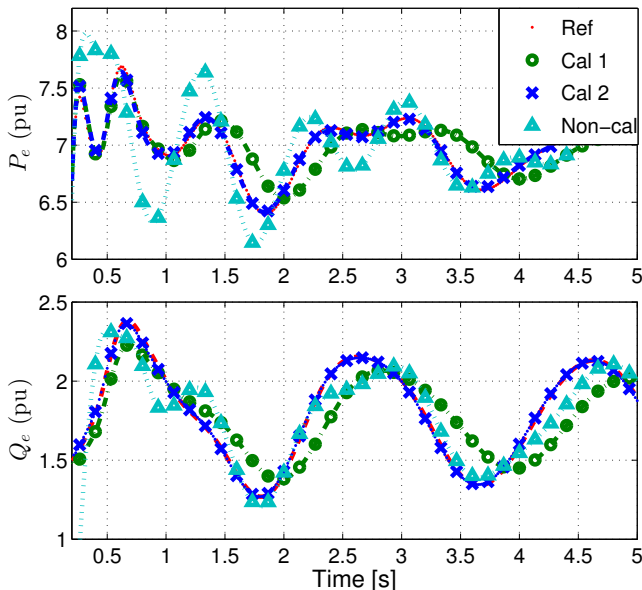


Fig. 7. Scenario B: Comparison among system outputs for different calibrations.

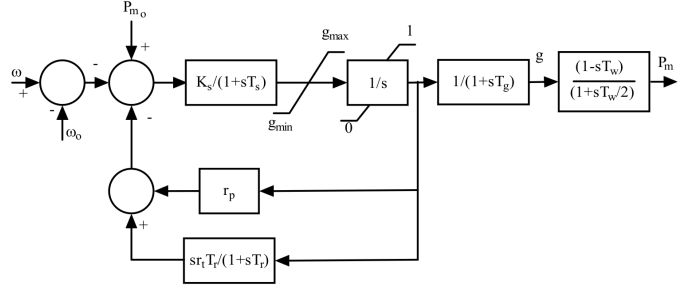


Fig. 8. Hydro turbine governor model.

have proposed to use knowledge of the voltage and current synchrophasors in conjunction with their time derivatives.

As it was mentioned in Section III-B, this approach takes advantage of the slow dynamics of the turbine governors. It is concluded that if the transition equations are based on the time derivative of the electric torque, the system is more robust and suitable for scenarios where the TG model is complex and only a coarse approximation of it is available. In turn, the TG model is simple and does not depend on a large number of parameters that are difficult to know a priori. In addition, the use of phasor derivatives allowed us to obtain a higher-order rotor dynamic model, which leads to an enhanced tracking of its state variables.

In Section IV, the results have shown that it is feasible to perform parameter estimation and a dynamic tracking of the state variables simultaneously. In particular, scenario B shows that poor performance is obtained when using a conventional model. This poor performance produces a considerable difference between the actual output of the system and the simulated one after the calibration process. This is an important fact, since a bad simulation of the system can lead to poor network planning. Furthermore, scenario C has shown decent results even though a complex hydro TG was used.

Finally, we would like to emphasize once again that this approach can be expanded and used with other estimation techniques, especially with different Bayesian filters where the application is immediate.

APPENDIX A COMPLEMENTARY EQUATIONS

In this appendix, we list the complementary equations of the model defined by (6b)-(9) and the expressions for additional model constants:

$$I_d = I_{re} \sin(\delta) - I_{im} \cos(\delta), \quad (36a)$$

$$I_q = I_{im} \sin(\delta) + I_{re} \cos(\delta), \quad (36b)$$

$$T_e = P_e + r_A (I_d^2 + I_q^2), \quad (36c)$$

$$E_d = \Psi_q'' - r_A I_d + x_d'' I_q, \quad (36d)$$

$$E_q = \Psi_d'' - r_A I_q - x_d'' I_d, \quad (36e)$$

$$V = \sqrt{E_d^2 + E_q^2}, \quad (36f)$$

$$S = k_{sat1} E_q'^2 + k_{sat2} E_q' + k_{sat3}. \quad (36g)$$

$$k_1 = \frac{(x_q - x'_q)(x'_q - x''_q)}{(x'_q - x_{ls})^2}, \quad k_2 = \frac{(x_q - x_{ls})(x''_q - x_{ls})}{(x'_q - x_{ls})},$$

$$k_3 = \frac{(x_d - x'_d)(x'_d - x''_d)}{(x'_d - x_{ls})^2}, \quad k_4 = \frac{(x_d - x_{ls})(x''_d - x_{ls})}{(x'_d - x_{ls})}.$$

APPENDIX B NOMENCLATURE

<i>Variables and constants [p.u.]</i>	
δ	Rotor angle.
ω	Angular velocity of the rotor.
$\dot{\omega}$	Time derivative of rotor velocity.
f	Instantaneous system frequency.
α	Instantaneous system ROCOF.
Ψ_d/Ψ_q	d/q axis subtransient voltage.
E'_d/E'_q	d/q axis transient voltage.
P_e/T_e	Active electric power / torque.
$P_m/P_{m,0}$	Instantaneous/Steady state mechanical power
E_{fd}	Field voltage.
I_d/I_q	d/q axis stator current.
V_{TR}	Transducer output signal.
pss	Power system stabilizer signal.
S	q-axis saturation function.
ω_0	Nominal rotor speed (1 p.u.)
r_A	Stator resistance
x_d, x_q	d/q axis synchronous reactance
x'_d, x'_q	d/q axis transient reactance
x''_d, x''_q	d/q axis sub-transient reactance
x_{ls}	Stator leakage reactance
T'_d, T'_q	d/q axis transient open circuit time constant
T''_d, T''_q	d/q axis subt-tran. open circuit time constant
k_{sati}	i-th core saturation factors
D	Damping factor
H	Inertia constant
$K_A/\frac{1}{r}$	Exciter/Turbine governor gain
T_R	Exciter time constant
T_{ef}	Turbine governor effective time constant
V_{REF}	Reference voltage of the excitation system

REFERENCES

- [1] A. Silverstein, E. Andersen, F. Tuffner, D. Kosterev, T. King, and J. D. Jr., "Model validation using phasor measurement unit data," NASPI North American Synchrophasor Initiative, Tech. Rep., 03 2015.
- [2] *Mandatory Standards Subject to Enforcement*, Std. North American Electric Reliability Corporation (NERC), 2017. [Online]. Available: <http://www.nerc.net/standardsreports/standardssummary.aspx>
- [3] *IEEE Guide for Synchronous Generator Modeling Practices and Applications in Power System Stability Analyses*, Std. 1110-2002 (Revision of IEEE Std. 1110-1991), 2003.
- [4] C. C. Tsai, L. R. Chang-Chien, I. J. Chen, C. J. Lin, W. J. Lee, C. C. Wu, and H. W. Lan, "Practical considerations to calibrate generator model parameters using phasor measurements," *IEEE Transactions on Smart Grid*, vol. 8, no. 5, pp. 2228–2238, Sept 2017.
- [5] J. J. Sanchez-Gasca, C. J. Bridenbaugh, C. E. J. Bowler, and J. S. Edmonds, "Trajectory sensitivity based identification of synchronous generator and excitation system parameters," *IEEE Transactions on Power Systems*, vol. 3, no. 4, pp. 1814–1822, Nov 1988.
- [6] M. Burth, G. C. Verghese, and M. Velez-Reyes, "Subset selection for improved parameter estimation in on-line identification of a synchronous generator," *IEEE Transactions on Power Systems*, vol. 14, no. 1, pp. 218–225, Feb 1999.
- [7] Z. Huang, P. Du, D. Kosterev, and B. Yang, "Application of extended kalman filter techniques for dynamic model parameter calibration," in *2009 IEEE Power Energy Society General Meeting*, July 2009, pp. 1–8.
- [8] H. G. Aghamolki, Z. Miao, L. Fan, W. Jiang, and D. Manjure, "Identification of synchronous generator model with frequency control using unscented kalman filter," *Electric Power Systems Research*, vol. 126, pp. 45 – 55, 2015.
- [9] R. Fan, Z. Huang, S. Wang, R. Diao, and D. Meng, "Dynamic state estimation and parameter calibration of a dfig using the ensemble kalman filter," in *2015 IEEE Power Energy Society General Meeting*, July 2015, pp. 1–5.
- [10] N. Zhou, D. Meng, Z. Huang, and G. Welch, "Dynamic state estimation of a synchronous machine using pmu data: A comparative study," *IEEE Transactions on Smart Grid*, vol. 6, no. 1, pp. 450–460, Jan 2015.
- [11] Z. Huang, P. Du, D. Kosterev, and S. Yang, "Generator dynamic model validation and parameter calibration using phasor measurements at the point of connection," *IEEE Transactions on Power Systems*, vol. 28, no. 2, pp. 1939–1949, May 2013.
- [12] E. Ghahremani and I. Kamwa, "Local and wide-area pmu-based decentralized dynamic state estimation in multi-machine power systems," *IEEE Transactions on Power Systems*, vol. 31, no. 1, pp. 547–562, Jan 2016.
- [13] J. Zhao, M. Netto, and L. Mili, "A robust iterated extended kalman filter for power system dynamic state estimation," *IEEE Transactions on Power Systems*, vol. 32, no. 4, pp. 3205–3216, July 2017.
- [14] J. C. K. W. Cheung and G. Rogers. Power system toolbox. [Online]. Available: http://www.eps.ee.kth.se/personal/vanfretti/pst/Power_System_Toolbox_Webpage/PST.html
- [15] P. Sauer and M. Pai, *Power System Dynamics and Stability*. Stipes Publishing L.L.C., 2006. [Online]. Available: <https://books.google.com.ar/books?id=yWi9PAAACAAJ>
- [16] C. C. Tsai, W. J. Lee, E. Nashawati, C. C. Wu, and H. W. Lan, "Pmu based generator parameter identification to improve the system planning and operation," in *2012 IEEE Power and Energy Society General Meeting*, July 2012, pp. 1–8.
- [17] *IEEE Standard for Synchrophasor Measurements for Power Systems*, IEEE Std. C37.118.1-2011 (Revision of IEEE Std C37.118-2005) Std., Dec 2011.
- [18] J. A. de la O Serna, "Dynamic phasor estimates for power system oscillations," *IEEE Transactions on Instrumentation and Measurement*, vol. 56, no. 5, pp. 1648–1657, Oct 2007.
- [19] D. Petri, D. Fontanelli, and D. Macii, "A frequency-domain algorithm for dynamic synchrophasor and frequency estimation," *IEEE Transactions on Instrumentation and Measurement*, vol. 63, no. 10, pp. 2330–2340, Oct 2014.
- [20] M. Bertocco, G. Frigo, C. Narduzzi, C. Muscas, and P. A. Pegoraro, "Compressive sensing of a taylor-fourier multifrequency model for synchrophasor estimation," *IEEE Transactions on Instrumentation and Measurement*, vol. 64, no. 12, pp. 3274–3283, Dec 2015.
- [21] F. Messina, L. R. Vega, P. Marchi, and C. G. Galarza, "Optimal differentiator filter banks for pmus and their feasibility limits," *IEEE Transactions on Instrumentation and Measurement*, vol. 66, no. 11, pp. 2948–2956, Nov 2017.
- [22] L. Vanfretti, S. Bengtsson, and J. O. Gjerde, "Preprocessing synchronized phasor measurement data for spectral analysis of electromechanical oscillations in the nordic grid," *International Transactions on Electrical Energy Systems*, vol. 25, no. 2, pp. 348–358, 2 2015.